THE INFLUENCE OF THERMOCLINE TOPOGRAPHY ON THE OCEANIC RESPONSE TO FLUCTUATING WINDS: A CASE STUDY IN THE TROPICAL NORTH PACIFIC

A. CAPOTONDI, M. A. ALEXANDER
NOAA-CIRES Climate Diagnostics Center
325 Broadway, R/CDC1, Boulder, CO 80305-3328

1. Introduction

Thermocline processes likely play an important role in climate variability at decadal timescales. Surface anomalies subducting at midlatitudes propagate in the main thermocline toward the tropics with a timescale close to decadal. Thermocline variability is also associated with baroclinic Rossby waves, a fundamental agent in the adjustment of the ocean circulation, whose propagation time can introduce a delay of several years in the oceanic feedback to atmospheric forcing.

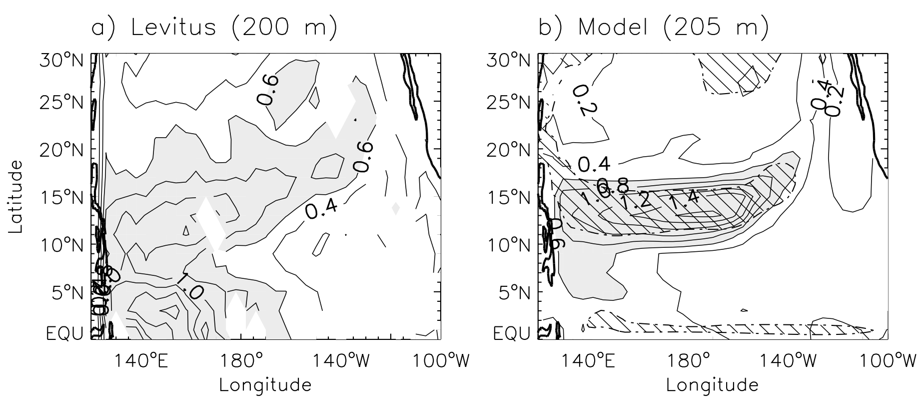

Figure 1.Temperature standard deviation at 200m depth in the Pacific using data from Levitus (a), and from a numerical model simulation performed with the NCAR ocean model forced with observed surface forcing over the period 1958-1997 (b). Contour interval is 0.2°C. Values larger than 0.6°C are shaded. In (b) the hatching indicates areas where the meridional gradients of the depth of the 15°C isotherm exceed 1.2×10^{-4}.

In the Pacific the thermocline exhibits three centers of variability, as indicated by temperature variance at 200m depth, one in the Kuroshio extension around 40°N, the second between 10°N and 15°N, and the third around 10°S. In this paper we will focus on the variability in the 10°–15°N latitude band (Figure 1). What is special about this region? Is

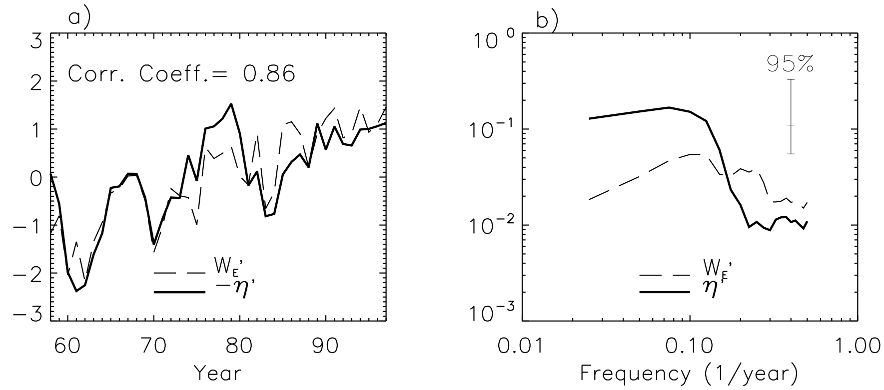

Figure 2. a) Time series of annual anomalies of Ekman pumping (dashed line) averaged over the area 179°E-140°W, 11°–14°N, and time series of the annual depth anomalies of the 25.5σ_θ isopycnal, with the sign reversed (thick solid line). The two time series are normalized to unit standard deviation. b) Spectra of the time series in a).

the enhanced variance associated with a stronger surface forcing, or is the ocean response more pronounced in this area? Capotondi and Alexander (2000, CA hereafter) have analyzed the variability at 10°–15°N using the results from the National Center for Atmospheric Research (NCAR) ocean General Circulation Model (GCM) (Gent et al. 1998) referred to in Figure 1b. CA have shown that the band of enhanced variance around 13°N is associated with Rossby waves forced by anomalous Ekman pumping east of approximately 180°, while west of this longitude the waves appear to be freely propagating. Although several aspects of the waves can be explained in terms of characteristics of the surface forcing, the reason for the particularly large variance in the 10°-15°N latitude band remains unclear. In this paper we examine the possibility that spatial changes in mean thermocline depth may be responsible for the amplitude of the oceanic response to variable wind forcing. We will see that meridional movements of the thermocline can account for a large fraction of the temperature variability at 13°N.
The paper is organized as follows: in section 2 we summarize the major findings of CA concerning the nature of the variability at 13°N, while in section 3 we examine the importance of the thermocline "topography" for determining the amplitude of the variability. We conclude in section 4.

2. Variability at 10°-15°N

2.1 THE OCEAN SIGNAL

Zonal sections of temperature and salinity anomalies along 13°N (CA) show that the largest amplitudes are found in the thermocline, and are associated with large changes in isopycnal depth, suggesting that the variability in this latitude band is primarily due to adiabatic movements of the thermocline. The time evolution of the 25.5 σ_θ depth anomalies is dominated by the low-frequencies (periods longer than ~ 7 years) as shown in Fig-

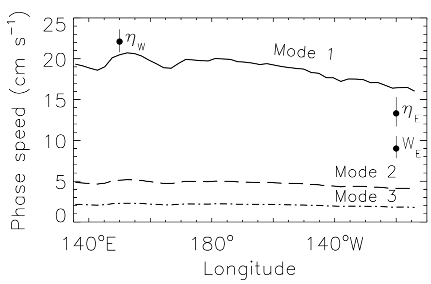

Figure 3. Phase speed of model baroclinic Rossby waves along 13.6°N, estimated using the WKB approximation. Dots indicate the phase speeds of the ocean signal and the Ekman pumping estimated from the model.

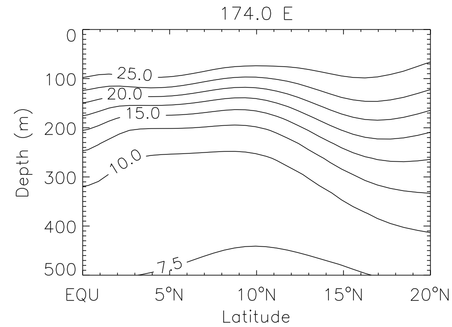

Figure 4. Meridional section of the time averaged temperature field in the model at 174°E. Contour interval is 2.5°C.

ure 2a, b, where the changes in thermocline depth are compared with the local Ekman pumping in a box centered at 160°W, 13°N. In addition to an upward trend in both time series, the ocean model has low-frequency variability, with a timescale close to 10 years (Figure 2a). The oceanic spectrum (Figure 2b) is redder than the spectrum of the forcing, with enhanced power at periods longer than ~7 years.

The propagation characteristics have been studied in CA using cross-spectral analysis. In the decadal range (7-10 years), the thermocline displacements along 13°N remain coherent, at the 90% significance level, with the thermocline displacements in the eastern end of the basin all the way to the western boundary. Significant coherence is also found along part of the western boundary, both to the north and south of 13°N, indicating that after reaching the boundary the incoming signal propagates along the boundary. The southern branch reaches the equator, and produces thermocline depth anomalies of 5-10m along the equator, with the potential of modulating ENSO on decadal timescales (Meehl et al. 2000, Fedorov and Philander 2000).

In the 7-10 years spectral band, phase lags increase monotonically from east to west. Phase speeds can be estimated by relating the phase lags between signals at different points to the distance between those points. It is found that in the eastern half of the basin the phase speed is ~13 cm s^{-1}, while west of the dateline the phase speed increases to ~22 cm s^{-1}, a value in agreement with previous observational estimates (Kessler 1990).

These results can be understood in the framework of Rossby wave dynamics. The phase speeds of the first three baroclinic Rossby wave modes have been estimated for the model using the WKB approximation (Morse and Feshbach 1953). The result along 13°N is shown in Figure 3. For the first baroclinic mode, the phase speed predicted by linear theory increases from about 15 cm s^{-1} close to the eastern boundary to ~20 cm s^{-1} in the western half of the basin, in agreement with the observational study of Chelton et al. (1998). Thus, the oceanic signal is slower than the first baroclinic Rossby wave mode east of the dateline (η_E in Figure 3), while west of the dateline it is slightly faster (η_W in Figure 3). The different propagation characteristics in the eastern and western halves of the basin can be understood by examining the nature of the forcing.

2.2 FORCING

Ekman pumping is the component of the surface forcing which can be expected to produce adiabatic thermocline displacements. For this model simulation, Ekman pumping is derived from the NCEP/NCAR reanalyses. Local correlations as large as 0.8 are found between Ekman pumping and changes in thermocline depth east of ~180°, while west of the dateline correlations drop to values smaller than 0.5. A direct comparison between the Ekman pumping and thermocline displacements time series is shown in Figure 2a, the correlation coefficient being 0.86. Cross-spectral analysis shows that east of the dateline Ekman pumping anomalies in the 7-10 year spectral band propagate westward with a phase speed of ~9 cm s^{-1} (indicated by W_E in Figure 3). Thus, we can interpret the ocean model signal east of the dateline as forced Rossby waves which propagate westward closely tracking the Ekman pumping anomalies. The westward propagation of "decadal" Ekman pumping anomalies with a phase speed which is very close to the phase speed of free Rossby waves (Figure 3) can explain the "decadal" timescale of the waves as a preferred response to the forcing in that frequency band. West of the dateline, on the other hand, thermocline variability mainly consists of free, first-mode baroclinic Rossby waves.

While the spectrum of the ocean signal can be explained in terms of the characteristics of the forcing, the amplitude of the ocean response around 13°N seems to be independent of propagating Ekman pumping anomalies. A preliminary analysis of a coupled integration performed with the NCAR climate model shows the presence of a similar band of enhanced thermal variance at 13°N, although the Ekman pumping characteristics in the coupled model appear to be different. Thus, the origin of the enhanced variance in that latitude band may be associated with the ocean structure.

3. Effects of thermocline topography

Figure 1b shows the presence of large meridional gradients in the depth of the 15°C isotherm (a proxi for thermocline depth comparable to the $25.5\sigma_\theta$ isopycnal) which closely overlap the band of enhanced thermal variance at 10°–15°N. At these latitudes, the thermocline deepens poleward (Figure 4), so that an equatorward displacement of the thermocline will result in a positive temperature anomaly for an observer sitting at a fixed point. The isotherms are almost parallel with a maximum slope achieved at ~13°N (Figure 4). The instantaneous position of the maximum meridional gradient can be used as an indicator of meridional displacements of the thermocline. An example of the evolution of that position is shown in Figure 5a for 174°W. The time series of temperature anomalies at 174°W, 13°N, 230m depth (the approximate depth of the 15°C isotherm at this point) is also shown on the same axis for comparison. Poleward displacements are associated with negative temperature anomalies, and vice versa, and the two time series are nearly opposite, with a correlation coefficient of -0.97.

What is the mechanism responsible for the meridional displacements, and how much of the signal can it account for? The evolution of the thermocline depth at a fixed point is governed by the equation

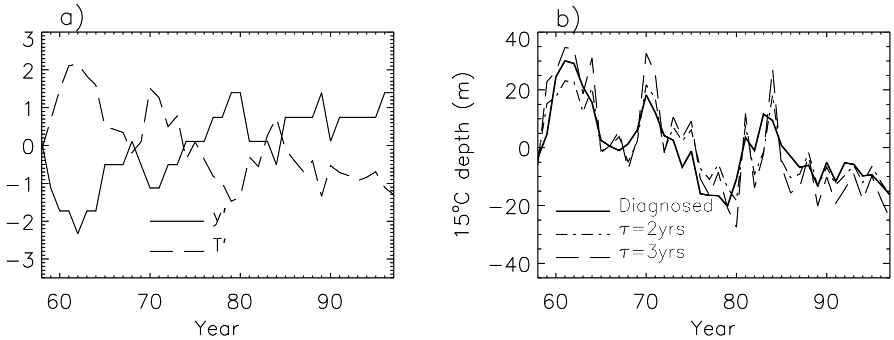

Figure 5. a) Time series of the position of the maximum meridional thermocline slope (y', solid line), and time series of temperature anomalies at 174°W, 13.6°N, 230 m depth (T', dashed line). Both time series are normalized to unit standard deviation. b) Time series of the depth anomalies of the 15°C isotherm diagnosed from the model in the box 180°–140°W, 9°–15°N (thick solid line), and computed from equation (4) in the same box for τ=2 years (dot-dashed line), and τ=3 years (dashed line). The correlation coefficient is 0.88 in both cases.

$$\frac{\partial\eta}{\partial t} = w - u\frac{\partial\eta}{\partial x} - v\frac{\partial\eta}{\partial y} - r\eta \qquad (1)$$

where η is the thermocline depth, u, v, and w are the zonal, meridional, and vertical components of the velocities, respectively, and r is the friction coefficient. Equation (1) says that at a fixed spatial point η changes can be due to vertical displacements of the isotherm, or to horizontal advection of depth gradients. At the long timescales we are considering (periods longer than ~7 years) dissipation can be important, and for simplicity we include it in the form of Rayleigh friction. Each variable can be decomposed in time mean and deviation components ($a=\bar{a}+a'$, where a is any of the variables, the overbar indicates the time mean, and the prime indicates the anomaly). After introducing this decomposition in Equation (1) and linearizing, we examine the relevance of the balance

$$\frac{\partial\eta'}{\partial t} \sim -v'\frac{\partial\bar{\eta}}{\partial y} - r\eta' \qquad (2)$$

for which changes in thermocline depth are primarily due to anomalous advection of the mean meridional gradient, where the anomalous velocity v' may be associated with the Rossby waves. If we assume an oscillatory time dependence for v' ($=v_o e^{i\omega t}$) the solution of Equation (2) will also be oscillatory ($\eta=\eta_o e^{i\omega t}$) with

$$\eta_o = -v_o\frac{\partial\bar{\eta}}{\partial y}\frac{(r - i\omega)}{(r^2 + \omega^2)} \qquad (3)$$

For periods much longer than the frictional timescale τ ($=1/r$), we have $\omega \ll r$, so that

$$\eta_o \sim -\tau v_o\frac{\partial\bar{\eta}}{\partial y} \qquad (4)$$

When friction is important, the amplitude of the response is in opposition of phase with the meridional advection, and increases with decreasing friction. Equation (4) is tested in the box 180°–140°W, 9°–15°N. The results are shown in Figure 5b, where the changes in the depth of the 15°C isotherm are compared with those predicted by (4) using the anomalous velocities obtained directly from the ocean model at the depth of the mean 15°C isotherm in the box. Frictional timescales of 2 and 3 years are considered. As a reference, the timescale estimated from the isopycnal eddy diffusion coefficient used in the model simulation (0.8×10^3 m^2 s^{-1}) and from the model zonal grid size (2.4°) is 2.7 years. The result shows that for reasonable values of the frictional timescale the anomalous meridional advection of mean thermocline slope can account for a large fraction of the thermocline depth variability in that box.

4. Conclusions

We have examined the effect of spatial variations of mean thermocline depth on the oceanic response to fluctuating winds. We have focused our analysis on a relatively narrow latitude band in the tropical North Pacific (~10°−15°N), where enhanced variability is found in the thermocline. The variability is associated with baroclinic Rossby waves forced by anomalous Ekman pumping in the eastern half of the basin.
The 10°−15°N band coincides with an area of large meridional gradients in mean thermocline depth. We have shown that anomalous meridional advection of those gradients is primarily responsible for the enhanced variability in that region. Thus, the vertical velocities directly induced by the Ekman pumping are not necessarily the dominant factor in determining the amplitude of the wave field, but the meridional advection of mean thermocline gradients by the anomalous velocities associated with the Rossby waves may play a fundamental role.

5. References

Capotondi, A. and Alexander, M. A. (2000) Rossby waves in the tropical North Pacific and their role in decadal thermocline variability, *J. Phys. Oceanogr.*, submitted.

Chelton, D. B., DeSzoeke, R. A., and Schlax, M. G. (1998) Geographical variability of the first baroclinic Rossby radius of deformation, *J. Phys. Oceanogr.*, **28**, 433-460.

Fedorov, A. V. and Philander, S. G. (2000) Is El Niño changing?, *Science*, **288**, 1997-2002.

Gent, P. R., Bryan, F. O., Danabasoglu, G., Doney, S. C., Holland, W. R., Large, W. G., McWilliams, J. C. (1998) The NCAR Climate System Model global ocean component, *J. Climate*, **11**, 1287-1306.

Kessler, W. S. (1990) Observations of long Rossby waves in the northern tropical Pacific, *J. Geophys. Res.*, **95**, 5183-5217.

Meehl, G. A., Gent, P. R., Arblaster, J. M., Otto-Bliesner, B. L., Brady, E. C., and Craig, A. (2000) Factors that affect the amplitude of El Niño in global climate models, *Climate Dyn.,* in press.

Morse, P. M., Feshbach, H. (1953) *Methods of theoretical physics*, McGraw-Hill.